Optics and Lasers in Engineering 166 (2023) 107568

Contents lists available at ScienceDirect

Optics and Lasers in Engineering

journal homepage: www.elsevier.com/locate/optlaseng

Evaluation of polymer-based eccentric FBG bending sensor for humidity, strain, temperature and torsion

Lennart Leffers[a,*], Bernhard Roth[a,b], Ludger Overmeyer[a,b,c]

[a] Hannover Centre for Optical Technologies, Gottfried Wilhelm Leibniz University Hanover, Nienburger Str. 17, Hannover 30167, Germany
[b] Cluster of Excellence PhoenixD, (Photonics, Optics, and Engineering-Innovation Across Disciplines), Hannover 30167, Germany
[c] Institute for Transport and Automation Technology, Gottfried Wilhelm Leibniz University Hanover, An der Universität 2, Garbsen 30823, Germany

ARTICLE INFO

Keywords:
Fiber Bragg gratings
Fiber optics
Optical bend sensor
Polymer optical fiber
Strain sensor
Temperature sensor
Torsion sensor
UV excimer laser

ABSTRACT

We analyse and evaluate the sensitivity and robustness of an eccentric fiber Bragg grating sensor micro-structured into a polymer optical fiber under different relative humidity, temperature, strain and torsion conditions. Relative humidity and temperature conditions are established with a climate test chamber and prepared salt solutions. Though made of polymer, the cross-sensitivity of the sensor to relative humidity is low, enabling usage in rapidly changing environment applications, e.g., for movement detecting gloves or in vehicles, but also in high moisture situations. We find a linear dependence on temperature, so that either bending or temperature can be measured separately from each other. After rotation of one end, the sensor measures torsion by observing the light intensity and the change of the full width at half maximum. Strain measurement shows multiple elastic strain regions before final plastic deformations occur. In the next step, the flexible sensor system will be implemented in a sensor glove to monitor finger movement and detect different hand gestures.

1. Introduction

In engineering, maximum temperature and humidity are crucial design parameters regarding operability and functionality of systems, machines and the sensor units contained therein. Under high temperature and humidity conditions and - in extreme cases - under water most electrical devices and sensors break irreparably due to short circuits. Both, glass and polymer optical fibers (POF) are very resistant to water and humid environments and are only slightly affected by them. Hence, they are excellent alternatives for electrical circuits and sensors. However, the relative humidity is not only a crucial design parameter to ensure the functionality of electrics, it is also a factor which is crucial for the long-term stability of components similar to mechanical stress. The latter, for example, leads to strain and torsion and the observation of these is constantly desired in key components nowadays. Fiber optical sensors (FOS) have already replaced electrical sensors since several years in an increasing number of applications, where temperature [1], relative humidity [2], strain [3], torsion [4], rotation [5], pressure [6], vibration [7], bending angle [8], bending radius [9–11] bending direction [12–14], a wide range of biological adhesions [15], chemical reactions [16] and many more [17–20] are measured. In addition, optical fibers provide not only good resistance to humidity, but also offer the advantages of a lower Young's modulus, higher elastic strain, higher ductile breaking limits, resistance to corrosion, insensitivity to electromagnetic interference [21] and a lower weight compared to their electrical counterparts. These advantages overcome existing disadvantages such as lower tensile strength, lower bend and torsion breaking limits and, in the case of POF, lower temperature resistance in many applications leading to an increase of not only the interest [22] but also the world-wide application of FOS [23] in all industrial fields. A large portion of these FOS is realized by the implementation of fiber Bragg gratings (FBGs). Usually, FBGs are periodic variations of the refractive index in an optical fiber, which are produced by femtosecond laser [24,25], holography [26] or phase-mask-method [9]. Another manufacturing approach is the die-press-print method, in which a microstructured stamp alternates the surface of the fiber(core) either by a mechanically induced transfer of the stamp's microstructure [27] or by adhesion of specific markers [28]. In sports, medicine and consumer electronics the share of wearable devices shows a continious growth in the recent years and especially polymer optical fiber Bragg gratings are under intensive research due to their light weight, high flexibility and lower cost compared to glass fibers. Smart wearables can observe the respiratory movement [29], the heart beat [30], the contraction of muscle-groups [31] and an associated joint motion or even pressure distributions in beds [32] and shoe insoles [33].

In this work, we evaluate the sensitivity of multimode POF sensors with inscribed eccentric FBGs with respect to the relative humidity, temperature, strain and torsion, which are the most relevant quantities to

* Corresponding author.
E-mail address: lennart.leffers@hot.uni-hannover.de (L. Leffers).

https://doi.org/10.1016/j.optlaseng.2023.107568
Received 29 November 2022; Received in revised form 17 February 2023; Accepted 3 March 2023
Available online 16 March 2023

affect such measurement devices and wearables containing them. The experimental validation is realized under controlled conditions. The results build the basis for utilization of such sensor systems in motion capture gloves, which we will implement in future work.

2. Theory and methods

Periodic refractive index (RI) modifications inscribed into optical fibers result in a wavelength specific reflection of a particular fraction of the broadband light spectrum propagated therein. The reflected Bragg wavelength is given by:

$$\lambda_B = 2 \cdot n_{eff} \cdot \Lambda, \tag{1}$$

where Λ is the periodicity of the refractive index and n_{eff} is the effective refractive index of the material after structuring, usually determined as $n_{eff} = \frac{n_1+n_2}{2}$. Here, n_1 and n_2 are the refractive indices of the unmodified and modified material of the fiber core.

A change of the physical state of the fiber affects either the periodicity Λ, the effective refractive index n_{eff} or both. For applied bending, relative humidity, temperature, strain or torsion this results in a shift of the Bragg wavelength:

$$\Delta\lambda_B = 2 \cdot \Sigma\left(n_{eff}\frac{d\Lambda}{di} + \Lambda\frac{dn_{eff}}{di}\right)\Delta i, \tag{2}$$

where i stands for the relative humidity RH, the temperature T, the bending b, the strain ε and the torsion τ [34]. Eq. (2) can be simplified to

$$\Delta\lambda_B = S_{RH} \cdot \Delta RH + S_T \cdot \Delta T + S_b \cdot \Delta b + S_\varepsilon \cdot \Delta\varepsilon + S_\tau \cdot \Delta\tau, \tag{3}$$

where S denotes the corresponding sensitivity coefficients for the above quantities [35]. For practical reasons it has to be noted, that the measurements of strain and torsion are destructive and are ideally not applied together with the measurement of bending, resulting in a simplified equation for bending measurements:

$$\Delta\lambda_B = S_{RH} \cdot \Delta RH + S_T \cdot \Delta T + S_b \cdot \Delta b. \tag{4}$$

The polymer optical fiber sensor itself is manufactured by chemically uncoating and uncladding a GigaPOF50-SR (Chromis Technologies) CYTOP-fiber with tetrahydrofuran (Carl Roth GmbH + Co. KG), which is then micro-structured by a UV-laser (Atlex FBG-300, ATL Lasertechnik GmbH) and a phase mask (Ibsen Photonics A/S; Phasemask Technology, LLC) to create eccentric FBGs [2,9]. With 15 Hz over 256 s the FBGs are inscribed into the outer region of the core over a length of 3 mm. The absence of coating and cladding generally leads to a lower mechanical robustness and to a higher flexibility. It offers the advantage, that the analyzed effects are only related to the fiber core and are not affected by cladding or coating. The optical measurement setup consists of an optical spectrum analyzer (OSA, Anritsu MS9740B), a broadband light source (Thorlabs SLS201 L/M), a 50:50-splitter (Thorlabs TM105R5F1B) and the sensor, as shown in Fig. 1. The micro-structured POFs are positioned in environments with specified humidity or temperature conditions during measurements. 3D printed grooves are guiding the FBG-structured fibers into different bending positions: a straight position, an upward and a downward bending position with curvature of $\pm 148.148\ m^{-1}$, bringing the eccentric FBGs in a state of compression and stretching, respectively. All measurements are performed 50 times and mean values and standard deviations are calculated. Strain and torsion measurements are carried out in straight fiber position (Fig. 2). For this purpose, one fiber end is fixed on a rotation stage, which is positioned on a linear translation stage while the other fiber end is fixed on a rigid stage. The investigated fiber length is 5 cm long. Measurements are performed 10 times and mean values and standard deviations are calculated as well. For all measurements the peak position of the Bragg wavelength and corresponding shifts are evaluated. Also, full width at half maximum (FWHM) and the light intensity at the Bragg wavelength peak are analysed.

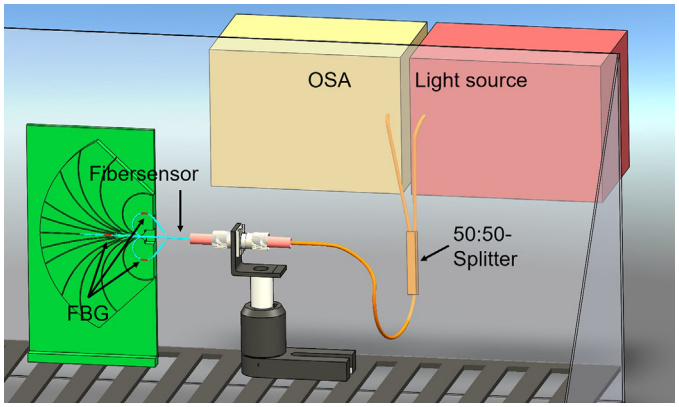

Fig. 1. Optical measurement setup to evaluate different bending positions under pre-set relative humidities or temperatures. The optical spectrum analyser (OSA), the light source and the 50:50-splitter are outside of a gas-tight test-chamber. The fiber sensor is displayed in three overlayed positions inside the 3D printed grooves. The position of the FBGs is marked in red. To measure different relative humidities the sensor is placed on a grid, under which an aqueous over-saturated salt solution is contained. (For interpretation of the references to color in this figure legend, the reader is referred to the web version of this article.)

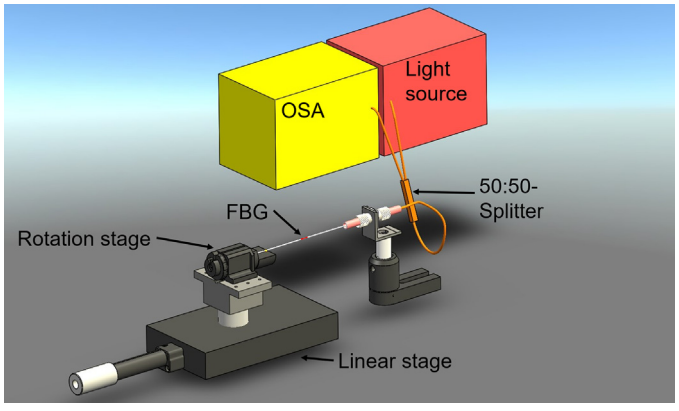

Fig. 2. Optical measurement setup to evaluate strain and torsion. The OSA, the light source and the 50:50-splitter are utilized to measure the FBG. The position of the FBG is marked in red. The sample is fixed on a rotation stage at one end, which is mounted on a linear translation stage. This setup is used for torsion or strain measurement, respectively. (For interpretation of the references to color in this figure legend, the reader is referred to the web version of this article.)

2.1. Humidity measurements

To achieve controlled relative humidity values, the following salts are used because of their defined relative humidity at equilibrium vapor pressure [36,37] : KOH, $MgCl_2$, $Mg(NO_3)_2$, $SrCl_2$, KCl, K_2SO_4. The respective values of the relative humidity for each over-saturated aqueous salt solution are shown in Fig. 3. For the measurements, the over-saturated solutions are filled into a sealed chamber Fig. 1, which also incorporates a hygrometer (Hygrometer testo 608-H1) to control the RH stability. To speed up the formation of an equally distributed vapor pressure inside the container a fan is installed, since the time of adjustment of the RH is otherwise only proportional to the gas diffusion constant and the volume of the sealed chamber. With an installed fan an equally distributed vapor pressure is achieved within a maximum time of three hours. All measurements are done under stable room temperature conditions of 21 °C.

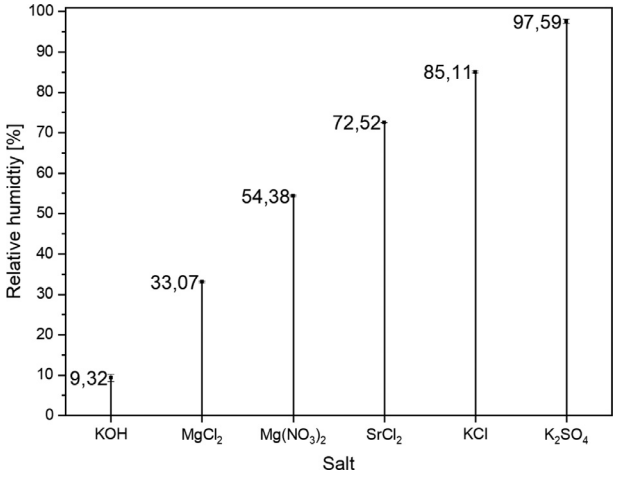

Fig. 3. Used salts and their relative humidity values in supersaturated aqueous solutions [37].

2.2. Temperature measurements

For measurements at different temperatures the samples are placed in a climate test chamber (Memmert GmbH & Co. KG, CTC256). Measurements are performed at 10 ± 1 °C, 20 ± 1 °C, 30 ± 1 °C and 40 ± 1 °C. At 50 °C or above no measurements are performed to exclude mechanical transformation of the fiber-core, as well as at 0 °C or below, due to unstable temperature conditions before achieving the equilibrium state and an associated formation of ice crystals which are breaking the connection between the fiber and the mechanical holders.

2.3. Strain measurements

Strain is applied to the 5 cm fiber section by moving the translation stage in increments of initially 0.01 mm and later 0.05 mm, yielding strain-increments of $\varepsilon = 0.002$ and $\varepsilon = 0.01$, respectively. Increments of $\varepsilon = 0.002$ are applied as long as the fiber is free of constrictions and significant elongation is detected. After each increment in strain the fiber and the associated measurement is brought into the initial position to check whether plastic deformation affected the FBG. After $\varepsilon = 3.0, 6.2$ and 9.6 the fiber was left in the zero strain position for 15 h.

2.4. Torsion measurements

The fiber is twisted by rotating one fiber end in increments of 15° until a full rotation is achieved. A reference measurement is performed at 0°. Each torsion measurement followed a measurement in which the rotation is turned back to 0° to check whether a remaining deformation affected the sensor. The sensor rested for 15 h with 0° rotation before the measurement at 285° to determine the presence of relaxation processes and the sensor rested again for 50 h with a rotation of 360° before and after a measurement to evaluate deformation over time. Index matching oil ($n_{eff} = 1.41$) is utilised in the setup to achieve better coupling efficiencies between the POF sensor ($n_{eff} = 1.34$) and the glass fiber splitter ($n_{eff} = 1.49$). Therefore, the light intensity differs greatly after the resting times and the light intensity is only evaluated until a torsion degree of 270°.

3. Results and discussion

To verify, that the investigated sensor works, bending measurements are initially performed in upward and downward bending positions with a curvature of $\pm 148.148\ m^{-1}$. The Bragg wavelength shifts in stretching and compression bending mode are 2.556 ± 0.075 nm and -1.333 ± 0.101 nm, respectively. The absolute shift in compression bending is smaller compared to the stretching mode, indicating that the neutral axis is not exactly in the geometrical middle of the bend fiber. Neutral axis is the term for an axis or plane along which no longitudinal stresses or strains occur. Figure 4 shows the FBG in the fiber core as well as on the fiber surface.

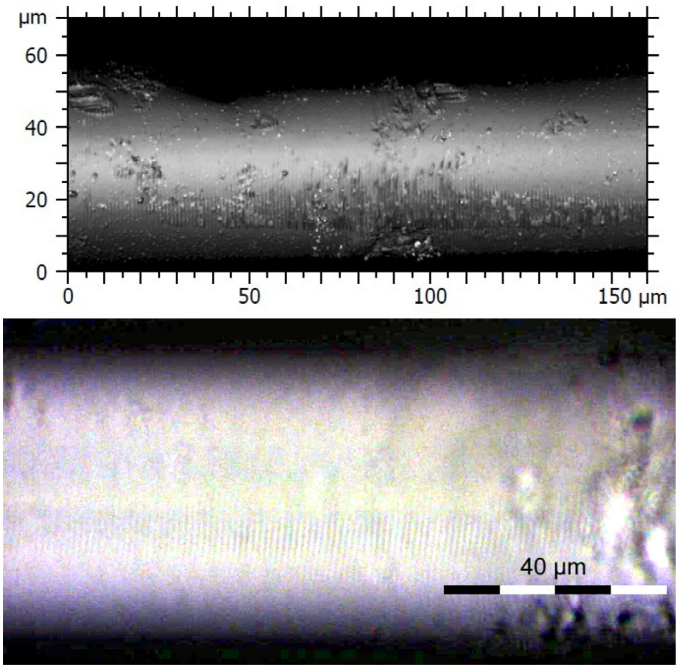

Fig. 4. Top: Confocal microscopy image of a fiber after the inscription process. The FBG is partially written into the surface of the fiber. Bottom: Transmitted-light microscopic image with focus in the fiber core.

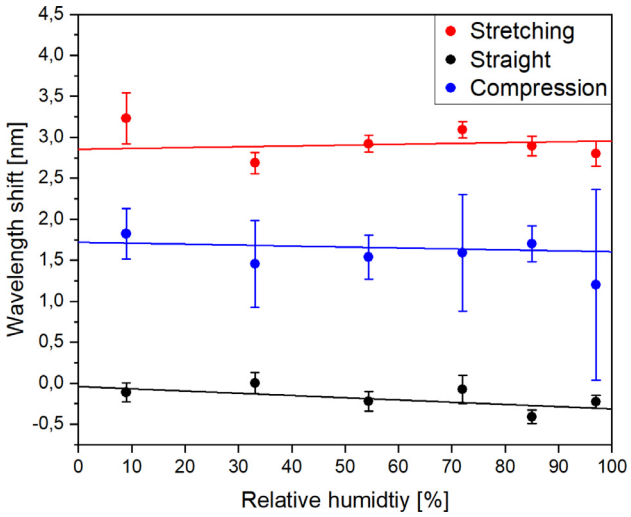

Fig. 5. Shift of the peak positions of the FBG in three different bending positions as function of the relative humidity. The straight measurement with 33.07% RH is used as reference. The corresponding regression lines show that there is only little dependence of the sensor to changes of RH. All measurements are performed at 21 °C.

3.1. Humidity measurement results

As shown in Fig. 5, it can be seen that the sensor exhibits very low sensitivity to changes of the relative humidity. Stretched, straight and compressed FBGs display low sensitivities of 1.01 $\frac{pm}{\%RH}$, -2.73 $\frac{pm}{\%RH}$ and

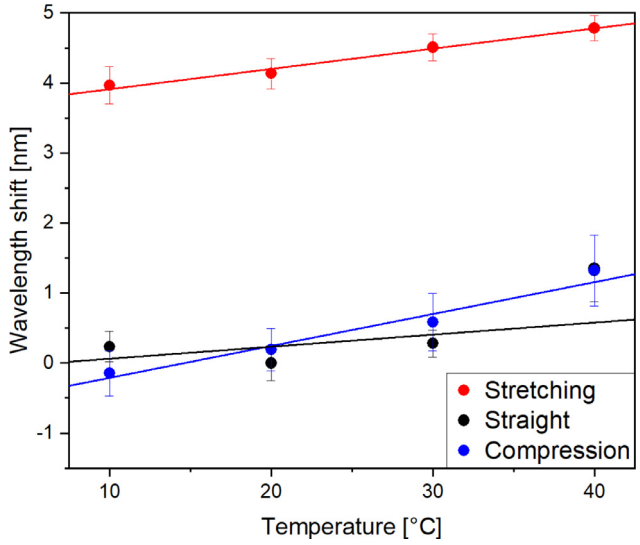

Fig. 6. Shift of the peak positions of the FBG in three different bending positions at four different temperatures. The straight measurement with 20 °C is used as reference. The corresponding regressions show a linear dependence of the Bragg wavelength with temperature.

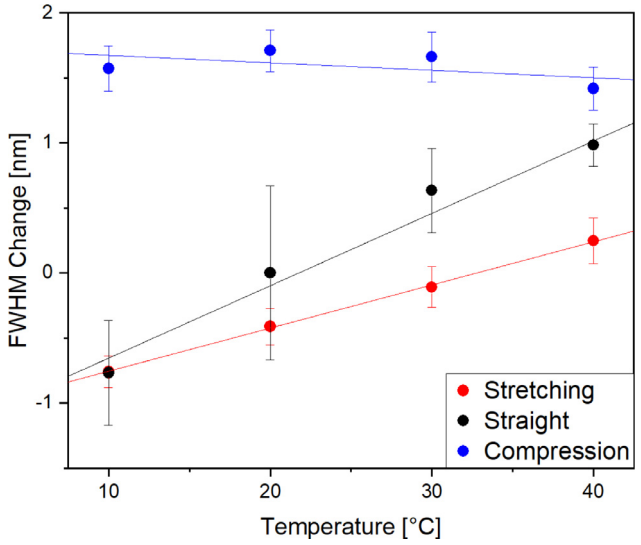

Fig. 7. Change of the FWHM of the FBG with temperature. The reference is defined at 20 °C in straight position.

$-1.16\ \frac{pm}{\%RH}$, respectively. This behavior is unexpected [38,39], since polymers usually take up water molecules and swell over time, and therefore a significant increase of the wavelength would be expected. From Eq. (2) it can be concluded, that either both relevant sensitivity coefficients are very small or one term cancels out the other. Any cross-sensitivity to relative humidity is therefore very low and negligible. It is to mention, that the Bragg wavelength shifts for the compression measurement are positive due to technical reasons, but the changes of the values and the sensitivity are not affected by this. Considering that the sensitivity to the relative humidity is negligible, Eq. (4) can again be simplified to:

$$\Delta\lambda_B = S_T \cdot \Delta T + S_b \cdot \Delta b. \tag{5}$$

3.2. Temperature measurement results

Even though the sensor is based on the polymer CYTOP, which has a negative thermo-optic coefficient of $\frac{dn}{dT} = -5 \times 10^{-5}\ \mathrm{K}^{-1}$ [40,41], the Bragg wavelength and the corresponding peak position rises proportionally with temperature (Fig. 6). This can be explained by the expansion coefficient of $7.4 \times 10^{-5}\ \mathrm{K}^{-1}$, outweighing the negative thermo-optic coefficient [2]. The grating constant of the FBG is increased more strongly and over-compensates the decrease of the refractive index with rising temperature, which leads to a red-shift of the Bragg-wavelength. The Bragg wavelength shifts for the bending measurements are higher than expected due to a relaxation process within the fiber, leading to a small change of the Bragg wavelength between the measurements in straight and bend positions. It is noticeable that for the different bending states different sensitivities are measured. In a straight position the peak of the Bragg wavelength shifts by a mean of 17.2 $\frac{pm}{K}$. The temperature sensitivities for the stretching and compression bending states are 28.94 $\frac{pm}{K}$ and 45.55 $\frac{pm}{K}$, respectively. This leads to the conclusion, that the thermal expansion coefficient is also affected by tensile or compressive stress in a discrete position in the fiber. The thermal sensitivity of the FBG in compression bending state is higher compared to the other states, which can be explained by a higher density of the molecules under compressive stress and therefore a higher dependence to the thermal expansion coefficient. On the other hand the FBG in stretched bending state also has a higher sensitivity compared to the straight FBG. This can be explained by a change of the thermo-optic coefficient with the change of the density of the material due to stretching [42,43]. With respect to these results the temperature sensitivity coefficient S_T needs to be modified, since it also depends on a factor for the bending state f(b):

$$S_T = 2 \cdot f(b) \cdot \left(n_{eff} \frac{d\Lambda}{dT} - \Lambda \frac{dn_{eff}}{dT} \right). \tag{6}$$

The values for the effective refractive index ($n_{eff} = 1.34$ [44], the thermo-optic and the expansion coefficients can be inserted into Eq. (6), so that one obtains a more specified temperature sensitivity coefficient for CYTOP:

$$S_T = 2 \cdot f(b) \cdot \left(n_{eff} \frac{\Lambda \cdot 7.4}{10^5\ \mathrm{K}} - \Lambda \frac{n_{eff} \cdot 5}{10^5\ \mathrm{K}} \right) \tag{7}$$

$$= 6.432 \cdot 10^{-5}\ \mathrm{K}^{-1} \cdot f(b) \cdot \Lambda. \tag{8}$$

This leads to a revision of Eq. (5):

$$\Delta\lambda_B = 6.432 \cdot 10^{-5}\ \mathrm{K}^{-1} \cdot f(b) \cdot \Lambda \cdot \Delta T + S_b \cdot \Delta b. \tag{9}$$

Considering a straight measurement without applied bending, the bending state factor f(b) is assumed to be 1 and the term $S_b \Delta b$ is equal to 0, which results in:

$$\Delta\lambda_B = 6.432 \cdot 10^{-5}\ \mathrm{K}^{-1} \cdot \Lambda \cdot \Delta T. \tag{10}$$

The FBGs grating constant in this experiment is 540 nm and when implemented into Eq. (10), this results in a gradient of $\Delta\lambda_B = 0.0347$ nm/K. This value is approximately twice the experimental value, which can be explained by constant outliers at 10 °C resulting in a poorly calculated slope ($R^2 = 0.29$). For the experimental stretching ($R^2 = 0.98$) and compression ($R^2 = 0.96$) experiments it is clear, that the bending state factor f(b) is positive for both bending directions, since both slopes are increased compared to the FBG in straight position but have the same bending radius. Therefore, the suggested bending state factor can be divided into one part for the bending curvature $f(b)_C$ and another part for the bending direction $f(b)_D$:

$$f(b) = f(b)_C + f(b)_D. \tag{11}$$

Figure 7 shows the change of the FWHM of the FBG peak in relation to the temperature. With increasing temperature the FWHM of the FBG peak of the fiber in straight position increases by $55.67 \pm 13.51\ \frac{pm}{K}$. When the fiber is bent the FWHM sensitivity to temperature decreases

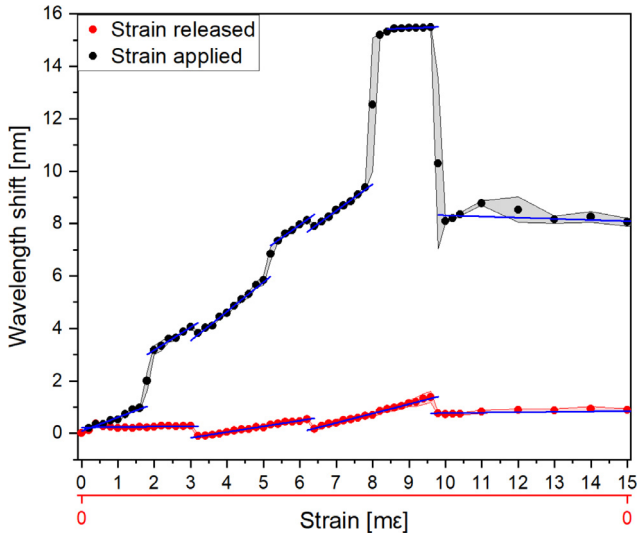

Fig. 8. The Bragg wavelength peak position shifts under the force of tensile stress (black) and relocated near to the initial position when the stress is unloaded (red). Blue lines show partial regressions of corresponding sections from left to right for applied strain: $0.524 \pm 0.043\ \frac{nm}{m\varepsilon}$, $0.871 \pm 0.133\ \frac{nm}{m\varepsilon}$, $1.115 \pm 0.048\ \frac{nm}{m\varepsilon}$, $0.990 \pm 0.113\ \frac{nm}{m\varepsilon}$, $1.013 \pm 0.056\ \frac{nm}{m\varepsilon}$, $0.057 \pm 0.057\ \frac{nm}{m\varepsilon}$, $-0.044 \pm 0.012\ \frac{nm}{m\varepsilon}$; and released strain: $0.014 \pm 0.017\ \frac{nm}{m\varepsilon}$, $0.220 \pm 0.006\ \frac{nm}{m\varepsilon}$, $0.357 \pm 0.025\ \frac{nm}{m\varepsilon}$, $0.014 \pm 0.005\ \frac{nm}{m\varepsilon}$. (For interpretation of the references to color in this figure legend, the reader is referred to the web version of this article.)

in the stretching bending state to $33.17 \pm 6.59\ \frac{pm}{K}$ and turns negative in compression bending state to $-5.75 \pm 7.64\ \frac{pm}{K}$. This supports other data from literature [1,45,46], where it was found that the temperature sensitivity of the FWHM values depend onto the sensitivities of wavelength shift and intensity variation. Despite this, in bending of eccentric FBGs it comes to a significant decrease of the temperature FWHM sensitivities. Especially the sensitivity in compression bending state turned negative, while the wavelength shift sensitivity was found higher compared to the others. Also, intensity sensitivity is not present in this specific case. This demonstrates that there is a relevant effect under bending conditions which can be explained by different mode groups affected by bending and that the former mentioned neutral axis of the bend fiber lies not in the middle but is shifted towards the inside of the bending.

3.3. Strain measurement results

The sensors sensitivity to strain is measured under pure tensile stress. As reported in the literature [47,48] the peak wavelength of the FBG increases with applied strain and decreases back, when the tensile stress is released. However, the presented sensor is made from the POF-material CYTOP, which exhibits a slightly different behavior under tensile stress compared to glass fibers. Under the load of tensile stress the sensor is strained and the FBG peak wavelength shifts into the red wavelength range. Due to the polymer material characteristics the material can strain-harden, which increases locally the resistance to strain and technically lowers the effective length of the strained material. This occurs for the in Fig. 8 shown sample at strains from 1.6 $m\varepsilon$ to 2 $m\varepsilon$; from 5 $m\varepsilon$ to 5.4 $m\varepsilon$ and from 7.8 $m\varepsilon$ to 8.2 $m\varepsilon$, where the Bragg wavelength shifts are larger than usual with respectively 2.21 nm; 1.495 nm and 5.824 nm. After strains of 3.2 $m\varepsilon$; 6.4 $m\varepsilon$ and 9.8 $m\varepsilon$ the shown sample rested for 15 h, resulting in an irreversible decrease of the wavelength shift, which is explained by a mechanically induced relaxation process in the fiber and is observable when strain is applied and unapplied. Initially, the measurements without applied strain are supposed to record irreversible changes to the FBG from previous applied strains, but also the relaxation is visible here. After the positive wavelength shift at 8 $m\varepsilon$ the ability to increase the wavelength of the FBG even further with strain

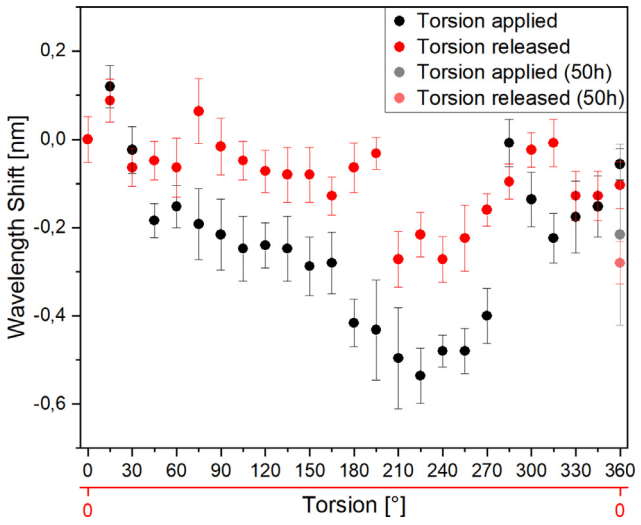

Fig. 9. Shift of the Bragg wavelength peak position under torsional stress. Sample points with released torsion (red) are set back to a rotation of 0°. Shifts are calculated from the first 0°-measurement. (For interpretation of the references to color in this figure legend, the reader is referred to the web version of this article.)

gets lost ($0.05710 \pm 0.05670\ \frac{nm}{m\varepsilon}$), explainable by constrictions in the fiber and resulting in damage of the sensor. Also the decrease of the shift after relaxation at 9.8 $m\varepsilon$ is bigger than before and the shift with applied strain does not increase afterwards but decreases ($-0.04441 \pm 0.01153\ \frac{nm}{m\varepsilon}$). This is also observed when the strain is not applied any more. Before the destruction of the sensor, the strain-sensitivity (Fig. 8, blue regression lines to corresponding black graph) increases slowly with increasing strain until a sensitivity of approximately $1\ \frac{nm}{m\varepsilon}$ is reached. This characteristic is typical for low temperature thermosoft plastics and is linked to their flow behavior under increasing strain load, which is supported by the irreversible changes and the as well increasing strain sensitivity without applied strain, showing the plastic deformation of the material. After resting for 15 h, the sensitivity is increased slightly compared to the sensitivity before resting, as long as the fiber has not taken any damage or a certain threshold (8.2 $m\varepsilon$) is exceeded. This is explained by the sensor being worn out while strain is applied and unapplied and again the relaxation process over 15 h is recovering the structural integrity partially, also leading to the mentioned decrease of the wavelength.

3.4. Torsion measurement results

Twisting the fiber over a length of 5 cm with increments of 15° results in a positive Bragg wavelength shift of 0.12 nm after 15°, in small negative shifts after 45° and in stronger negative shifts after 180° of torsion (Fig. 9). The decreasing shift with increasing torsion is a new effect and stands in contrast to the existing literature about fiber torsion [18,49]. The effect can only be explained by the eccentricity of the FBG, since direction dependent polarization effects in the sensor are not observed and the fiber material was examined with centric FBGs under torsion before [49]. The measurements with 285° and 360° torsion are performed as described in Subsection II-D. It is clearly visible, that the wavelength shift changed completely to the respective previous measurements. After a break of 15 h at 0° the Bragg wavelength shifted by only $8 \pm 53\ pm$ compared to the reference measurement. This can be explained by a relaxation of damage in the molecular structure of the fiber material induced by torsion, which is applied relatively fast but needs comparatively more time for relaxation which in turn affects the whole macromolecular structure of the sensor. Therefore this relaxation can only be measured after a few hours. After a pause of 50 h the measurement at 360° is repeated. The shift changed from $-56 \pm 35\ pm$

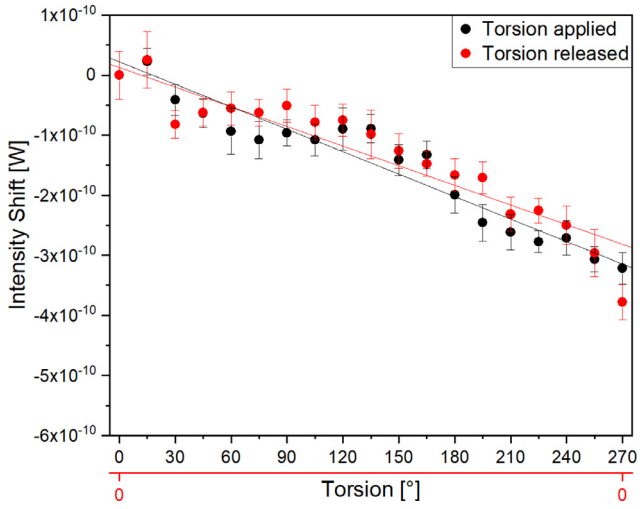

Fig. 10. Shift of the Bragg wavelength peak intensity under torsional stress. After the torsion measurement the sample is rotated back and measured at 0° (red marks). Shifts are calculated from the first 0°-measurement. A decrease of signal intensity is observed for measurements with and without torsion applied. Corresponding regressions show the linear dependence of the intensity to (formerly) applied torsion. (For interpretation of the references to color in this figure legend, the reader is referred to the web version of this article.)

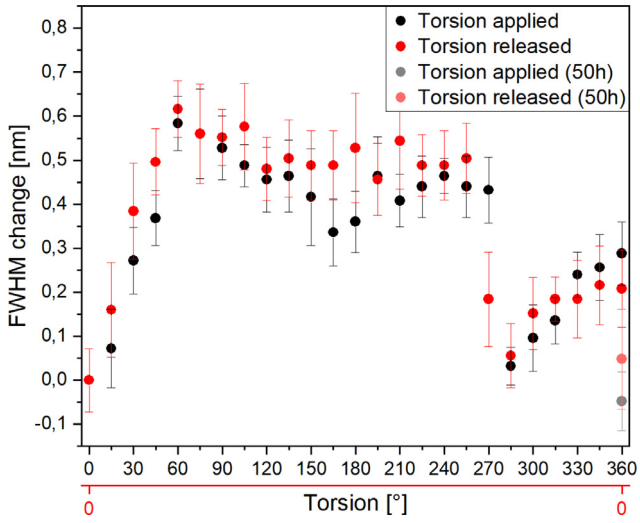

Fig. 11. Changes of the FWHM under torsional stress. Red marks show the FWHM when torsion is turned back again and changes are calculated from the first 0° measurement. (For interpretation of the references to color in this figure legend, the reader is referred to the web version of this article.)

to $-216 \pm 205\ pm$. This indicates, that the sensor over-compensates the damage by torsion deformation, when relaxation effects and torque are present. Also, the increase of the standard deviation in this measurement is significant, indicating a loss in the structural stability of the sample.

After a first small and negligible rise the light intensity at the peak position decreases continuously (Fig. 10) for both measurements with and without applied torsion. The torsion sensitivity of the intensity is $-1.248 \pm 0.074\ pW/°$ with applied torsion and $-1.091 \pm 0.081\ pW/°$ after release of the torsional stress, indicating with a constant and not recoverable loss in signal intensity above a certain torsion. This effect indicates that the fiber is facing irreversible damage under torsional stress. This offers the possibility to verify a torsion greater than 30° within the sensor, when the measured Bragg peak intensity is permanently reduced.

In Fig. 11 the change of the FWHM with applied torsion is shown. It can be observed, that the FHWM increases immediately after a small torsion is applied and that, even when the torsion is turned back, the FWHM still develops a further increase for a short time. After a torsion of 60° the FWHM change goes into saturation and remains more or less stable. After a pause of 15 h without applied torsion and after a pause of 50 h with applied torsion the FWHM recovers. This recovery is partially linked to the observation regarding the wavelength shift.

4. Conclusion

In this research, we evaluated a polymer-based fiber optic sensor with inscribed eccentric FBGs under various temperature and humidity conditions in different states of bending and under strain and torsional load. Destructive measurements with torsion and strain can be distinguishably measured by evaluating the Bragg wavelength and the peak intensity. The Bragg wavelength shifts to the red wavelength range under the load of tensile stress resulting in a strain, whereas under torsion, along with a steady decrease of the light intensity, the wavelength shifts into the blue. This offers usage of the sensor in a one-time critical defect detection in structural health monitoring of buildings [50] but also in the observation of more sensitive structural elements for example in production plants, systems and vehicles or even single screws to observe torque overload. The sensor shows no distinctive reaction to a change of the relative humidity opening a wide field of applications such as in maritime and tropical ambients, where high relative humidities or even liquids are preventing, complicating or interfering the usage of other technologies. A temperature change causes a proportional change in the Bragg wavelength and in the FWHM of the Bragg peak and can be determined by the combination of both. In smart configuration of multiple sensors the temperature can be separated by referencing and matrix calculations from the bending state of the sensor. These results enable the sensor to measure multiple different influences and build a good basis for vector bending sensing applications. In the future, we will utilize the sensor in a data glove system to capture motion and read out gestures to support working fields like intralogistics [51]. Also, other applications for the sensor are possible such as in augmented and virtual reality applications, in medical applications [52] such as endoscopes [53], in continuum robots [54] or wearable devices [29,33].

Funding

Funded by the Deutsche Forschungsgemeinschaft (DFG, German Research Foundation (OV 36/43-1)). B. Roth and L. Overmeyer acknowledge funding from the Deutsche Forschungsgemeinschaft (DFG, German Research Foundation) under Germany's Excellence Strategy within the Cluster of Excellence PhoenixD (EXC 2122, Project ID 390833453).

Declaration of Competing Interest

The authors declare that they have no known competing financial interests or personal relationships that could have appeared to influence the work reported in this paper.

Data availability

Data will be made available on request.

Supplementary material

Supplementary material associated with this article can be found, in the online version, at doi:10.1016/j.optlaseng.2023.107568.

References

[1] Leal-Junior A, Frizera-Neto A, Marques C, Pontes MJ. Measurement of temperature and relative humidity with polymer optical fiber sensors based on the induced stress-optic effect. MDPI Sens 2018;18(916):1–12. doi:10.3390/s18030916.

[2] Zheng Y, Bremer K, Roth B. Investigating the strain, temperature and humidity sensitivity of a multimode graded-index perfluorinated polymer optical fiber with Bragg grating. MDPI Sens 2018;18(1436):1–10. doi:10.3390/s18051436.

[3] Luo Y, Yan B, Li M, Zhang X, Wu W, Zhang Q, et al. Analysis of multimode POF gratings in stress and strain sensing applications. Opt Fiber Technol 2011;17(3):201–9. doi:10.1016/j.yofte.2011.02.005.

[4] Zhang W, Kai G, Dong X, Yuan S, Zhao Q. Temperature-independent FBG-type torsion sensor based on combinatorial torsion beam. IEEE Photonics Technol Lett 2002;14(8):1154–6. doi:10.1109/LPT.2002.1022000.

[5] Sartiano D, Sales S, Roca ET. Three lobes plastic optical fiber bending and rotation sensor. MDPI Proc 2019;15(15):1–5. doi:10.3390/proceedings2019015015.

[6] Bremer K, Reinsch T, Leen G, Roth B, Lochmann S, Lewis E. Pressure, temperature and refractive index determination of fluids using a single fibre optic point sensor. Sens Actuators, A 2017;256:84–8. doi:10.1016/j.sna.2017.01.025.

[7] Li C, Yang W, Wang M, Yu X, Fan J, Xiong Y, Yang Y, Li L. A review of coating materials used to improve the performance of optical fiber sensors. MDPI Sens 2020;20(4215):1–24. doi:10.3390/s20154215.

[8] Leal-Junior A, Theodosiou A, Díaz C, Marques C, Pontes MJ, Kalli K, et al. Polymer optical fiber Bragg gratings in cytop fibers for angle measurement with dynamic compensation. MDPI Polym 2018;10(674):1–16. doi:10.3390/polym10060674.

[9] Leffers L, Locmelis J, Bremer K, Roth B, Overmeyer. Optical bend sensor based on eccentrically micro-structured multimode polymer optical fibers. IEEE Photonics J 2021;13(5):1–7. doi:10.1109/JPHOT.2021.3111298.

[10] Chen X, Zhang C, Webb DJ, Kalli K, Peng G-D. Highly sensitive bend sensor based on Bragg grating in eccentric core polymer fiber. IEEE Photonics Technol Lett 2010;22(11):850–2. doi:10.1109/LPT.2010.2046482.

[11] Hu X, Chen X, Liu C, Mégret P, Caucheteur C, editors. D-shaped polymer optical fiber Bragg grating for bend sensing. Proceedings of advanced photonics, vol. SeS2B.5; 2015.

[12] Zhang H, Wu Z, Shum PP, Wang R, Dinh XQ, Fu S, et al. Fiber Bragg gratings in heterogeneous multicore fiber for directional bending sensing. J Opt 2016;18(085705):1–7. doi:10.1088/2040-8978/18/8/085705.

[13] Yang K, He J, Liao C, Wang Y, Liu S, Guo K, et al. Femtosecond laser inscription of fiber Bragg grating in twin-core few-mode fiber for directional bend sensing. J Lightwave Technol 2017;35(21):4670–6. doi:10.1109/JLT.2017.2750407.

[14] Bao W, Sahoo N, Sun Z, Wang C, Liu S, Wang Y, et al. Selective fiber Bragg grating inscription in four-core fiber for two-dimension vector bending sensing. Opt Express 2020;28(18):26461–9. doi:10.1364/OE.398794.

[15] Sypabekova M, Amantayeva A, Vangelista L, González-Vila Á, Caucheteur C, Tosi D. Ultralow limit detection of soluble her2 biomarker in serum with a fiber-optic ball-tip resonator assisted by a tilted FBG. ACS Meas Sci Au 2022;2(4):309–16. doi:10.1021/acsmeasuresciau.2c00008.

[16] Samavati Z, Samavati A, Ismail AF, Abdullah MS, Othman MHD. Selective ultrasensitive FBG-SBL chemosensor for detection of copper ions in water resources based on plasmon resonance energy transfer. Opt Laser Technol 2022;153(108289). doi:10.1016/j.optlastec.2022.108289.

[17] Hong C, Zhang Y, Lu Z, Yin Z. A FBG tilt sensor fabricated using 3D printing technique for monitoring ground movement. IEEE Sens J 2019;19(15):6392–9. doi:10.1109/JSEN.2019.2908873.

[18] Yi X, Chen X, Fan H, Shi F, Cheng X, Qian J. Separation method of bending and torsion in shape sensing based on FBG sensors array. Opt Express 2020;28(7):9367–83. doi:10.1364/OE.386738.

[19] Shadab A, Raghuwanshi SK, Kumar S. Advances in micro-fabricated fiber Bragg grating for detection of physical, chemical, and biological parameters—A review. IEEE Sens J 2022;22(16):15650–60. doi:10.1109/JSEN.2022.3188813.

[20] Zhu T, Loyez M, Chah K, Caucheteur C. Partially gold-coated tilted FBGs for enhanced surface biosensing. Opt Express 2022;30(10):16518–29. doi:10.1364/OE.458548.

[21] Peters K. Polymer optical fiber sensors—A review. Smart Mater Struct 2011;20(013002):1–17. doi:10.1088/0964-1726/20/1/013002.

[22] Budinski V, Donlagic D. Fiber-optic sensors for measurements of torsion, twist and rotation: a review. MDPI Sens 2017;17(443):1–29. doi:10.3390/s17030443.

[23] Allwood G, Wild G, Hinckley S. Fiber Bragg grating sensors for mainstream industrial processes. MDPI Electron 2017;6(92):1–19. doi:10.3390/electronics6040092.

[24] Martinez A, Lai Y, Dubov M, Khrushchev IY, Bennion I. Vector bending sensors based on fibre Bragg gratings inscribed by infrared femtosecond laser. Electron Lett 2005;41(8):472. doi:10.1049/el:20058278.

[25] Lacraz A, Polis M, Theodosiou A, Koutsides C, Kalli K. Femtosecond laser inscribed Bragg gratings in low loss cytop polymer optical fiber. IEEE Photonics Technol Lett 2015;27(7):693–6. doi:10.1109/LPT.2014.2386692.

[26] Battiato JM, Kostuk RK. 45 slanted fibre Bragg grating design with prism coupled holographic exposure. Electron Lett 2002;38(22):1323–4.

[27] Poulin J, Kashyap R. Novel fabrication of fiber Bragg gratings using silicone rubber phase-mask stamp on the cladding. J Lightwave Technol 2009;27(24):5602–6. doi:10.1109/JLT.2009.2033015.

[28] Juste-Dolz A, Delgado-Pinar M, Avella-Oliver M, Fernández E, Pastor D, Andrés MV, et al. Bio Bragg gratings on microfibers for label-free biosensing. Biosens Bioelectron 2021;176:112916. doi:10.1016/j.bios.2020.112916.

[29] Witt J, Narbonneau F, Schukar M, Krebber K, de Jonckheere J, Jeanne M, et al. Medical textiles with embedded fiber optic sensors for monitoring of respiratory movement. IEEE Sens J 2012;12(1):246–54. doi:10.1109/JSEN.2011.2158416.

[30] Tavares C, Leitão C, Lo Presti D, Domingues MF, Alberto N, Silva H, et al. Respiratory and heart rate monitoring using an FBG3D-printed wearable system. Biomed Opt Express 2022;13(4):2299–311. doi:10.1364/BOE.452115.

[31] Hong C-Y, Abro ZA, Zhang Y-F, Lakho RA. An FBG-based smart wearable ring fabricated using FDM for monitoring body joint motion. J Ind Text 2021;50(10):1660–73. doi:10.1177/1528083719870204.

[32] Hao J, Jayachandran M, Kng PL, Foo SF, Aung Aung PW, Cai Z. FBG-based smart bed system for healthcare applications. Front Optoelectron China 2010;3(1):78–83. doi:10.1007/s12200-009-0066-0.

[33] Domingues MF, Tavares C, Leitão C, Frizera-Neto A, Alberto N, Marques C, et al. Insole optical fiber Bragg grating sensors network for dynamic vertical force monitoring. J Biomed Opt 2017;22(9):91507. doi:10.1117/1.JBO.22.9.091507.

[34] Sousa I, Pereira L, Mesquita E, Souza VL, Araújo WS, Cabral A, et al. Sensing system based on FBG for corrosion monitoring in metallic structures. MDPI Sens 2022;22(5947):1–16. doi:10.3390/s22165947.

[35] Rocha M, Tavares C, Nepomuceno C, Da Antunes PFC, de Fatima Domingues M, Alberto NJ. FBGs based system for muscle effort monitoring in wheelchair users. IEEE Sens J 2022;22(13):12886–93. doi:10.1109/JSEN.2022.3177889.

[36] Wexler A, Hasegawa S. Relative humidity-temperature relationships of some saturated salt solutions in the temperature range 0 degree to 50 degrees c. J Res Natl Bur Stand 1954;53(1):19–25.

[37] Greenspan L. Humidity fixed points of binary saturated aqueous solutions. J Res Natl Bur Stand Sect A 1977;81A(1):89–96. doi:10.6028/jres.081A.011.

[38] Correia S, Antunes P, Pecoraro E, Lima PP, Varum H, Carlos LD, et al. Optical fiber relative humidity sensor based on a FBGwith a di-ureasil coating. MDPI Sens 2012;12(7):8847–60. doi:10.3390/s120708847.

[39] Woyessa G, Nielsen K, Stefani A, Markos C, Bang O. Temperature insensitive hysteresis free highly sensitive polymer optical fiber Bragg grating humidity sensor. Opt Express 2016;24(2):1206–13. doi:10.1364/OE.24.001206.

[40] Takenobu S, Kuwana Y, Takayama K, Sakana Y, Ono M, Sato H, Keil N, Brinker W, Yao H, Zawadtki C, Morizawa Y, Grote N, editors. All-polymer 8 × 8 AWG wavelength router using ultra low loss polymer optical waveguide material (CYTOP). Proceedings of the optical fiber communication conference/national fiber optic engineers conference, vol. JWA32; 2008.

[41] Fan H, Berini P. Thermo-optic characterization of long-range surface-plasmon devices in cytop. Appl Opt 2013;52(2):162–70. doi:10.1364/AO.52.000162.

[42] Moretti L, de Stefano L, Rossi AM, Rendina I. Dispersion of thermo-optic coefficient in porous silicon layers of different porosities. Appl Phys Lett 2005;86(061107):1–3. doi:10.1063/1.1857077.

[43] Johnson DI, Town GE. Photonics: design, technology, and packaging II: refractive index and thermo-optic coefficient of composite polymers at 1.55 μm. In: Proc. SPIE, vol. 6038; 2005.

[44] Ishigure T, Koike Y, Fleming JW. Optimum index profile of the perfluorinated polymer-based gi polymer optical fiber and its dispersion properties. J Lightwave Technol 2000;18(2):178–84. doi:10.1109/50.822790.

[45] Hisham HK. Full width-half maximum characteristics of FBG for petroleum sensor applications. Iraqi J Electr Electron Eng 2020;16(1):99–103. doi:10.37917/ijeee.16.1.12.

[46] Tahhan SR, Ali MH, Al-Ogaidi MAZ, Abass AK. Impact of apodization profile on performance of fiber Bragg grating strain–temperature sensor. J Commun 2019;14(1):53–7. doi:10.12720/jcm.14.1.53-57.

[47] Havermann D, Mathew J, MacPherson WN, Maier RRJ, Hand DP. Temperature and strain measurements with fiber Bragggratings embedded in stainless steel 316. J Lightwave Technol 2015;33(12):2474–9. doi:10.1109/JLT.2014.2366835.

[48] Guan B-O, Tam H-Y, Chan HLW, Choy C-L, Demokan MS. Discrimination between strain and temperature with a single fiber Bragg grating. Microw Opt Technol Lett 2002;33(3):200–2. doi:10.1002/mop.10275.

[49] Leal-Junior AG, Theodosiou A, Diaz CR, Marques C, Pontes MJ, Kalli K, et al. Simultaneous measurement of axial strain, bending and torsion with a single fiber Bragg grating in cytop fiber. J Lightwave Technol 2019;37(3):971–80. doi:10.1109/JLT.2018.2884538.

[50] Bremer K, Weigand F, Zheng Y, Alwis LS, Helbig R, Roth B. Structural health monitoring using textile reinforcement structures with integrated optical fiber sensors. MDPI Sens 2017;17(345):1–12. doi:10.3390/s17020345.

[51] Overmeyer L, Podszus F, Dohrmann L. Multimodal speech and gesture control of AGVs, including eeg-based measurements of cognitive workload. CIRP Ann - Manuf Technol 2016;65(1):425–8. doi:10.1016/j.cirp.2016.04.030.

[52] Mishra V, Singh N, Tiwari U, Kapur P. Fiber grating sensors in medicine: current and emerging applications. Sens Actuators, A 2011;167(2):279–90. doi:10.1016/j.sna.2011.02.045.

[53] Khan F, Denasi A, Barrera D, Madrigal J, Sales S, Misra S. Multi-core optical fibers with Bragg gratings as shape sensor for flexible medical instruments. IEEE Sens J 2019;19(14):5878–84. doi:10.1109/JSEN.2019.2905010.

[54] Xu R, Yurkewich A, Patel RV. Curvature, torsion, and force sensing in continuum robots using helically wrapped FBG sensors. IEEE Robot Autom Lett 2016;1(2):1052–9. doi:10.1109/LRA.2016.2530867.